A contribution to the baroclinic instability problem

By R. V. GARCIA and R. NORSCINI, *World Meteorological Organisation, Geneva, Switzerland*

(Manuscript received October 30, 1969; revised version February 20, 1970)

ABSTRACT

The problem of the baroclinic instability of zonal flow is formulated under assumptions similar to Green's model. The dynamic equations of the model lead to a single differential equation for the vertical velocity, which is of the confluent hyper-geometric type. The eigen-value problem is solved and numerical methods are only used to find the roots of the characteristic equation.

It is shown that, for large values of the nondimensional shear Λ (which is related to Green's parameter $\gamma = 2\Lambda^{-1}$), there is a continuous transition from fast growing unstable modes to unstable modes with small growth-rate. The eigen-values of the characteristic equation of the model do not show the continuous transition from the conjugate complex roots to the real roots as appears in the numerical computations of Green (1960) and Hirota (1968). On the other hand, for smaller values of the shear, a continuous transition from the unstable to stable solutions can occur. On the long wave side of such a transition point there are weak unstable waves whose steering level is *outside* the flow; on the short wave side there is a slight gap in the spectrum of unstable waves.

The structure of the waves is discussed and it is shown that the unstable waves with slow growth rate have the structure of a baroclinically unstable wave in a shallow layer close to the lower boundary.

1. Introduction

The well-known solutions found by Charney (1947) and Eady (1949) to the problem of baroclinic instability of a zonal flow were analyzed by Green (1960). He studied numerical solutions of a model which combined the essential characteristics of both Charney's and Eady's models. Green's model includes the latitudinal variation of Coriolis parameter (as in Charney's) and an upper rigid boundary (as in Eady's).

Green's analysis shows that for values of $\beta(\partial u/\partial z) > 0$ one of Eady's neutral solutions (the short neutral mode with steering level in the lower layer of the fluid) becomes unstable and therefore there is no short wave limit for the instability region of the wave spectrum. These short unstable waves are not found in two-layer models which have been studied by several authors. An explanation of this difference was given by Bretherton (1967*a*). In Bretherton (1967*b*) it is shown that the presence of a critical layer in which the phase speed of the perturbation is equal to the speed of the basic flow prevents the existence of (non singular) neutral modes.

Green's model has been studied more recently by Hirota (1968), again by numerical methods. He compared the different solutions obtained when the number of layers used for the computation is modifed. He finds that the number of critical curves of vanishing growth rate increases with the number of layers.

Parallel to the above investigations, Burger (1962) has shown, analytically, the existence of unstable solutions for wavelengths longer than Charney's critical wavelength and proved that there is no upper limit for the long unstable waves. Similar results were found by Miles (1964 *a*, *b*) who suggested a distinction between two types of instabilities which he calls "strong" and "weak" instabilities, the latter being associated to the presence of a critical layer.

The present paper contains an analysis of Green's model. The dynamic equations describing the behaviour of the model are combined into a single equation for the vertical speed, which turns out to be of the confluent hypergeometric type. The general solution can therefore be studied in detail. Numerical methods are only required for the adjustment of the general solution to the boundary conditions..

The results we have found confirm and extend

Green's and Hirota's results. There are, however, certain discrepancies which seem to be introduced by the finite-difference scheme they have used.

2. The model

The basic features of the model coincide with Green (1960). They are:

(i) Horizontal rigid surfaces at the upper and lower boundaries;

(ii) Adiabatic motion and incompressible and inviscid fluid;

(iii) A constant latitude variation of the Coriolis parameter;

(iv) Small values of the Rossby number ($R_0 = U_0/fL < 1$) and large values of the Richardson number ($R_i = \sigma g h^2/U_0^2 \gg 1$).

The basic flow is a constant vertical shear flow and the middle level will be our reference level. The east–west surface wind of the basic flow will have speed U_0. The west–east upper top wind will have the same speed.

We shall use the following symbols:

H	depth of the atmospheric layer
h	$H/2$
U_0	speed of the basic flow at the bottom and the top of the layer
ΔU	$2U_0$
$U(z)$	$U_0 z/h$ speed of the basic flow
u	zonal velocity component
v	meridional velocity component
w	vertical velocity
θ	potential temperature
g	acceleration of gravity
f	Coriolis parameter
k	wave number
C_r	phase velocity
$c_r = C_r/U_0$	dimensionless phase velocity
β	df/dy
$\zeta = \partial v/\partial x$	vertical component of the relative vorticity
$\sigma = \dfrac{1}{\bar\theta}\dfrac{\partial\bar\theta}{\partial z}$	static stability
$\mu = \dfrac{(\sigma g)^{\frac{1}{2}}}{U_0/h}$	square root of the Richardson number

3. The dynamical equations

The equation of motion, taking into account the geostrophic approximation and written as in the thermal wind equation, is:

$$f\frac{dv}{dz} = \frac{\partial \varkappa}{\partial x}, \tag{3.1}$$

where we have defined $\varkappa = g \ln \theta$. It is assumed that the motion is independent of y.

The vorticity equation, for the scale of motion in which we are interested, can be written:

$$\frac{D\zeta}{Dt} + \beta v = -f\frac{\partial u}{\partial x} \tag{3.2}$$

The thermodynamic equation, under the assumption of adiabatic motions, is $D\theta/Dt = 0$. Introducing the parameter $\varkappa$, we obtain:

$$\frac{D\varkappa}{Dt} - fv\frac{dU}{dz} + \sigma g w = 0 \tag{3.3}$$

Finally we have the continuity equation:

$$\frac{\partial u}{\partial x} + \frac{\partial w}{\partial z} = 0 \tag{3.4}$$

4. The confluent hypergeometric equation and the boundary conditions

We assume harmonic perturbations in the x-direction

$$(u, v) \sim \exp\,[ik(x - Ct)],$$

where $C = C_r + iC_i$ is the complex phase velocity.

From (3.1) to (3.4) we can write the perturbation equations:

$$\frac{\partial v}{\partial z} = \frac{1}{f}\frac{\partial \varkappa}{\partial x}, \tag{4.1}$$

$$\frac{\beta}{kf}v - \frac{k}{f}(U - C)\,v - \frac{1}{k}\frac{\partial w}{\partial z} = 0, \tag{4.2}$$

$$\frac{1}{f}(U - C)\frac{\partial \varkappa}{\partial x} - v\frac{dU}{dz} + \frac{\sigma g}{f}w = 0 \tag{4.3}$$

Defining $\xi = 2\mu k f^{-1}(U - C)$, where μ represents the square root of the Richardson number, and introducing in the equations (4.2) and (4.3), we obtain:

$$\left(\frac{\xi}{2} - \alpha\right)v + \frac{\mu}{k}\frac{\partial w}{\partial z} = 0 \tag{4.4}$$

in which $\alpha = \mu\beta/kf$, and:

$$\frac{\xi}{2}\frac{\partial \varkappa}{\partial x} - k\mu\frac{dU}{dz}v + \frac{\sigma g k}{f}\mu w = 0 \qquad (4.5)$$

From the last two equations we can obtain the perturbation differential equation of the vertical velocity:

$$\xi(\xi - 2\alpha)\frac{d^2 w}{d\xi^2} - 2(\xi - \alpha)\frac{dw}{d\xi} - \frac{1}{4}(\xi - 2\alpha)^2 w = 0 \qquad (4.6)$$

If we now introduce the transformation:

$$w = p - \xi\frac{dp}{d\xi}, \quad \text{where} \quad p = \frac{\xi}{2}e^{-\xi/2}\phi(\xi), \qquad (4.7)$$

the equation (4.6) is transformed into the confluent hypergeometric equation:

$$\xi\phi'' + (2 - \xi)\phi' - a\phi = 0, \qquad (4.8)$$

where the primes indicate differentiation with respect to ξ, and:

$$a(k) = 1 - \frac{\alpha}{2} = 1 - \frac{\mu\beta}{2kf} \qquad (4.9)$$

The general solution of (4.7) is the linear combination:

$$\phi = A\varphi(a, 2, \xi) + B\Psi(a, 2, \xi), \qquad (4.10)$$

where:

$$\varphi(a, c, \xi) = 1 + \frac{a}{c}\xi + \frac{a(a+1)}{c(c+1)}\frac{\xi^2}{2!} + \dots \qquad (4.11)$$

$$\Psi(a, 2, \xi) = \frac{1}{\xi\Gamma(a)} + \frac{1}{\Gamma(a)}\sum_{m=0}^{\infty}\left[\frac{\Gamma(a+m)}{\Gamma(a-1)\,m!\,(m+1)!}\right]$$
$$\times[\ln\xi + \psi(a+m) - \psi(1+m) - \psi(2+m)]\xi^m \qquad (4.12)$$

In the last series, ψ is the logarithmic derivative of the gamma function.

The general solution (4.10) must satisfy the boundary condition that the vertical velocity vanishes at the rigid boundaries. This condition can be obtain from (4.7):

$$w = \tfrac{1}{4}\xi^2 e^{-\xi/2}[\phi(a, \xi) - 2\phi'(a, \xi)] \qquad (4.13)$$

which becomes $w = 0$ for the values of ξ:

$$\begin{cases} \xi = \xi_t = \dfrac{2\mu k}{f}(U_0 - C) & (z = h) \\[2ex] \xi = \xi_b = -\dfrac{2\mu k}{f}(U_0 + C) & (z = -h) \end{cases}$$

From (4.13) and (4.10) two linear and homogeneous equations in A and B result, so the determinant of the coefficients must vanish:

$$[\varphi(a, \xi_t) - 2\varphi'(a, \xi_t)]\,[\Psi(a, \xi_b) - 2\Psi'(a, \xi_b)]$$
$$-[\varphi(a, \xi_b) - 2\varphi'(a, \xi_b)]\,[\Psi(a, \xi_t) - 2\Psi'(a, \xi_t)] = 0 \qquad (4.14)$$

When a is a negativ integer or zero the series (4.11) and (4.12) are not linearly independent solutions. In that case one solution is given by the associated Laguerre polynomial and the other linearly independent solution may be calculated by the Wronskian method.

5. The characteristic-value problem and the numerical treatment

If we take the wavelength λ and the vertical shear Λ in the dimensionless forms:

$$\lambda = \frac{f}{(\sigma g)^{\frac{1}{2}} hk} = \frac{f}{\mu U_0 k} \qquad (5.1)$$

$$\Lambda = \frac{f^2}{\sigma g h}\frac{U_0}{h\beta} = \frac{f^2}{\mu^2 U_0 \beta} \qquad (5.2)$$

the parameter $\alpha = \mu\beta/kf$ defined in (4.4) becomes:

$$\alpha = \frac{\lambda}{\Lambda} \qquad (5.3)$$

so, in the diagram in which λ and Λ are the coordinates, the lines along which α is constant are straight lines. Along these lines the series φ and Ψ (4.11 and 4.12) are functions of ξ only, and (4.14) is the equation for determining the characteristic values.

As ξ is a complex variable and can be expressed as:

$$\xi = X - iX_i = \frac{2\mu k}{f}(U - C) \qquad (5.4)$$

the real and imaginary parts are:

$$X = \frac{2\mu k}{f}(U - C_r) \quad (5.5)$$

$$X_i = \frac{2\mu k}{f} C_i \quad (5.6)$$

At the boundaries the real part takes the values:

$$X_t = \frac{2\mu k}{f}(U_0 - C_r) \quad (z = h) \quad (5.7)$$

$$X_b = -\frac{2\mu k}{f}(U_0 + C_r) \quad (z = -h) \quad (5.8)$$

We have found numerically those values of X_i, X_t and X_b that satisfy equation 4.14 along the lines α constant.

The complex phase velocity and the wavelength may be determined from the values of X_i, X_t, X_b which satisfy the characteristic equation. By combination of (5.7), (5.8) and (5.1) we obtain:

$$X_t - X_b = \frac{4}{\lambda} \quad (5.9)$$

$$X_t + X_b = -c_r \frac{4}{\lambda} \quad (5.10)$$

where $c_r = C_r/U_0$. From these relations the dimensionless phase velocity results:

$$c_r = -\frac{X_t + X_b}{X_t - X_b} \quad (5.11)$$

When the thermal wind of the basic flow is westerly, as in our model ($U' > 0$), equation (4.14) contains no solutions for values of X_t and X_b outside the ranges

$$X_t > 0$$

$$-X_t \leqslant X_b \leqslant X_t$$

It follows from (5.11) that $c_r < 0$. All waves are, therefore, retrograde waves, with reference to a system in which the air at the central level is at rest. These waves have a phase velocity greater than the speed of the surface wind when X_b is positive, and smaller than the surface wind when X_b is negative. Obviously when $X_b = 0$ the retrograde waves have the same speed as the surface wind.

From the values of X_i, X_t, X_b we can also obtain the expresion of the dimensionless growth rate:

$$n = \frac{f}{\mu\beta\Delta U} kC_i = \frac{X_i}{\alpha(X_t - X_b)} \quad (5.12)$$

6. The neutral solutions

The neutral solutions are found when we assign real values to the variable ξ. When $X_i = 0$, the remaining imaginary part of equation (4.14), due to the logarithmic term in the series Ψ, does not vanish simultaneously with the real part for any negative value of X_b. Neutral waves must therefore satisfy the conditions

$$X_t > 0$$

$$0 \leqslant X_b \leqslant X_t \quad (6.1)$$

In a diagram with coordinates X_t, X_b all neutral-wave solutions can be represented as isolines of constant α. They are curves contained in the sector limited by the straight lines $X_b = X_t$ and $X_b = 0$. We have drawn two such diagrams. Fig. 1 shows some neutral-wave curves for small values of α, up to 2.1. Fig. 2 has an expanded X_t scale and shows neutral-wave curves for two arbitrarily selected larger values of α($\alpha = 7$ and $\alpha = 9.5$). In both diagrams any straight line through the origin is a line of constant speed. In view of (5.11) and (6.1) all values of the phase velocity are within the range

$$-\infty \leqslant c_r \leqslant -1$$

This means that the neutral modes never reach the speed of the flow at any level. There are, therefore, no neutral waves with steering level within the flow. This result differs from Hirota's (1968).

The curves represented in Figs. 1 and 2 have the following features. Firstly, when α is small, there is only one branch for each value of α (Fig. 1); as α increases, the number of branches for each value of α also increases (Fig. 2 shows three branches for $\alpha = 7$ and four branches for $\alpha = 9.5$). The transition from one branch to two or more branches was found numerically to occur at $\alpha = \alpha' \approx 3.3$. Secondly, for values of $\alpha < 2$ all curves end at $X_b = X_t$ and $X_b = 0$. It follows from (5.9) that the wavelengths of the corresponding neutral waves are bounded:

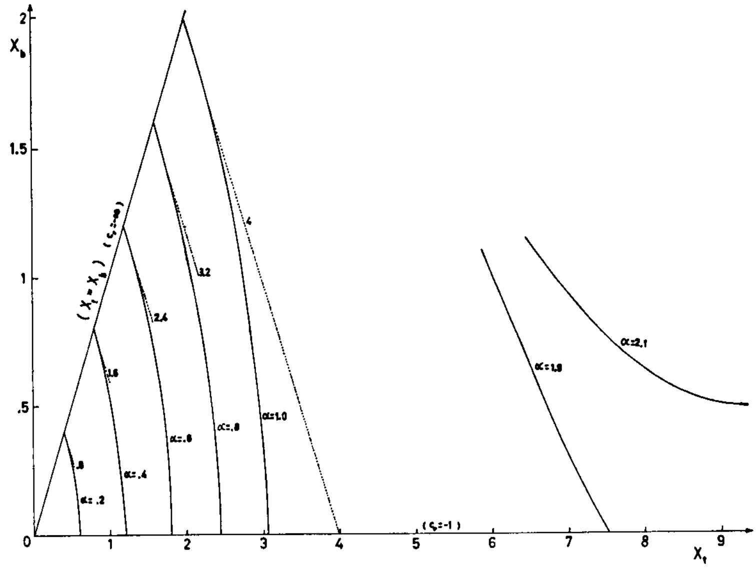

Fig. 1. Neutral solutions for several constant (small) values of α. Dotted lines: isopleths of $X_t + X_b$.

$$\frac{4}{X_t} \leqslant \lambda \leqslant \infty$$

For $\alpha > 2$ the curves have one branch which does not intersect the X_t axis and the wavelength can therefore have any value.

It should be finally pointed out that Eady's neutral solutions ($\alpha = 0$) would be located in our diagrams in the region $X_b < 0$, $X_t > 0$. We cannot reach these solutions asymptotically since X_b remains positive when $\alpha \to 0$.

Let us now see how the spectrum of neutral modes is distributed in a λ, Λ diagram (Fig. 3). According to (5.3) the lines $\alpha = \text{const}$ (or $a = \text{const}$) are straight lines through the origin. We have noted that for small values of α the wafe-

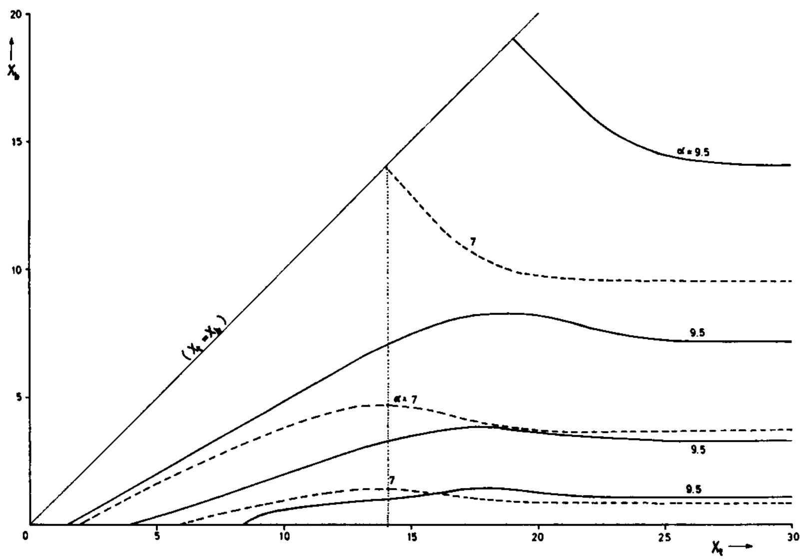

Fig. 2. Typical cases of neutral solutions for larger values of α.

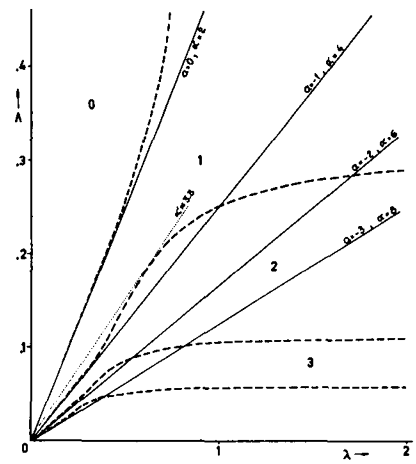

Fig. 3. Spectrum of neutral modes. Dashed lines: critical neutral solutions with phase velocity $c_r = -1$. The figures indicate the number of neutral roots in each point λ, Λ of the regions bounded by the critical neutral lines.

lengths of the neutral modes have a lower bound

$$\lambda_c = \frac{4}{X_t}$$

The corresponding values of X_t are found by the following method.

Because of the singularity of the logarithmic term of the series $\Psi(a, 2, X_b)$ defined in (4.12) for $X_b = 0$, the values of X_t are determined by the roots of:

$$F(a, X_t) = X_t^2 \exp(-X_t/2)\,[\varphi(a, 2, X_t) - 2\varphi'(a, 2, X_t)] = 0 \qquad (6.2)$$

For the values of a which are neither a negative integer nor zero, $\varphi(a, 2, X_t)$ is the series defined in (4.11). For the small values of a (let us say $a < \frac{1}{2}$; i.e. $\alpha < 1$), the roots of (6.2) satisfy the approximate relation $X_t \approx 3\alpha$. With this relation and (5.9) we obtain:

$$\Lambda = \tfrac{2}{3}\lambda_c^2 \quad (\alpha < 1) \qquad (6.3)$$

Thus, for large nondimensional shears this parabola bounds the region where neutral solutions exist (dashed line in Fig. 3). There are no neutral solutions for any wavelengths which have $\lambda < \lambda_c$. This limiting parabola agrees with the limit found by Green (1960). When $\alpha \to 2$ (small shears) the parabola degenerates into a line approaching asymptotically the straight line $\alpha = 2$ $(a = 0)$ (Fig. 3).

We can see in Fig. 2 that for large values of $\alpha(\alpha > \alpha')$ more than one branch of solutions reaches the limit line $X_b = 0$. This means that the parabola is not the unique line of neutral solutions with phase velocity $c_r = -1$. In fact we can see in Fig. 3 several lines representing the locus of the critical values which correspond to neutral modes which propagate with phase velocity $c_r = -1$.

When $\lambda \to 0$, $\Lambda \to 0$ these critical lines show an interesting feature: they become respectively asymptotic to the straight lines $a = -1$, $a = -2$, ..., etc., in the same manner as the parabola (6.3) did with respect to the straight line $a = 0$. These asymptotic lines correspond to Burger's singular curves (Burger, 1962) (Miles 1964 *c*). On the other hand, the generic straight line $a = -n$ $(n = 0, 1, 2, ...)$ has n intersections with the critical lines (see Fig. 3). In fact, for the negative integers or zero values of a the series φ in the condition (6.2) is defined by the associated Laguerre polynomials:

$$\varphi(-m, 2, X_t) = \frac{1}{m+1} L_m^1(X_t)$$

$$(a = -m;\ m = 0, 1, 2, \ldots)$$

$$L_m^1(X_t) = \sum_{r=0}^{m} \binom{m+1}{m-r} \frac{(-X)^r}{r!}$$

$F(-m, X_t)$ will have a number of roots equal to the degree of the Laguerre polynomial.

We wish to call attention in particular to the critical line of neutral solutions which tend asymptotically to the straight line $a = -1$ $(\alpha = 4)$ when $\lambda \to 0$, $\Lambda \to 0$. This line is the boundary of two regions in which the roots behave differently, as it is explained below. We sall *a*-region the region limited by this neutral line and the Λ-axis, and *b*-region the region limited by the neutral line and the λ-axis (see Fig. 3).

Inside the *a*-region, as we have already said, there are no neutral roots for the values of $\lambda < \lambda_c$ (6.3), and there is only one neutral root for every value of $\lambda \geq \lambda_c$. Inside the *b*-region there are subregions whose boundaries are the set of critical neutral lines we have defined. In these subregions there is an increasing number of neutral solutions for each point (λ, Λ). The numbers in Fig. 3 indicate the number of roots at each point within each subregion. These numbers are obviously the counterpart, in the λ, Λ diagram, of the number of branches for each α in the X_b, X_t diagram (Figs. 1 and 2).

On each critical line (boundaries of subregions) which is asymptotic at the origin to the straight line $a = -m$ (m = non negative integer), the number of neutral solutions is $m+1$ (i.e. the number of neutral roots at each point of the neighbouring subregion counted clockwise).

Turning back to Figs. 1 and 2, it can be seen that for every value of α there are always solutions such that

$$X_t > 2\alpha$$

and

$$X_b < 2\alpha$$

It follows that the term $\alpha - (X/2)$ of equation (4.4) changes its sign with height. There is, therefore, one level at which

$$\alpha - \frac{X}{2} = \frac{\mu k}{f}\left(\frac{\beta}{k^2} - U_c + C_r\right) = 0$$

or

$$C_r = U_c - \frac{\beta}{k^2},$$

i.e. the waves propagate like Rossby waves relative to the flow at this level. Equation (4.4) also shows that this is the level of no-divergence. This level of no-divergence changes from point to point on the same α-line. It is interesting to notice that each α-line, as it approaches the limiting value $X_b = X_t$, becomes asymptotic to the straightlines (dotted lines in Figs. 1 and 2):

$$X_t + X_b = 4\alpha$$

or, from (5.10)

$$X_t + X_b = -\frac{4}{\lambda}\frac{C_r}{U_0}$$

When this relation is combined with (5.1), (5.2) and (5.3) we obtain the Rossby phase velocity

$$C_r = -\frac{\beta}{k^2}$$

The level of no-divergence is therefore at the central level of the basic flow.

When $\alpha > \alpha' \approx 3.3$ there are branches (Fig. 2) with segments in a region such that $X_t < 2\alpha$ and $X_b < 2\alpha$. They represent solutions where the term $\alpha - (X/2)$ is positive at all levels. In these cases the change in the sign which results from equation (4.4) is due to the change in the sign of v with height. These modes propagate with phase velocities

$$U - \frac{\beta}{k^2} < C_r \leqslant -U_0 \qquad (6.4)$$

Applying now the above results to the distribution of the spectrum in Fig. 3 we find that neutral modes in the a-region are all Rossby type waves. On the other hand, in the b-region there are also neutral modes moving with the speed (6.4). Furthermore, an analysis of the vertical structure of the waves shows that the neutral waves in the a-region have no nodal planes. In the b-region one finds waves of more complex structure. The first b-subregion has waves without nodal planes and waves with one nodal plane in the v-field. As one moves from one sub-region to the next (clockwise) one finds new waves with an additional nodal plane. Obviously there are, in addition, nodal planes for the w-field which are easily found from (4.4)

7. The unstable solutions

When the variable ξ takes complex values ($X_i \neq 0$) the solutions correspond to exponentially unstable modes. For almost all wavelengths we found two conjugate complex solutions of the characteristic equation (4.14). This pair of roots corresponds to an amplifying and a decaying mode. We have shown in Fig. 4, for some constant values of the parameter α, the curves representing unstable solutions. We have selected different scales for both axes in order to expand the region in which we are interested. The line $X_t = -X_b$ (which is also $C_r = 0$) corresponds to the limiting case $\alpha = 0$ which corresponds to unstable solutions in Eady's model. The numbers on each line are values of X_i, which are related to the growth rate by the relation (5.12). It can be seen that the unstable waves with the fastest growth rates shift toward the short wavelengths when α increases. On the other hand, in the shortest wavelengths, for $\alpha \neq 0$, unstable roots appear with slow growth rates which have an asymptotic tendency toward one branch of the Eady's neutral roots when $\alpha \to 0$. This portion of the curves cannot be shown in Fig. 4 because we have used an expanded scale for X_b in order to show some other new features. The asymptotic behaviour

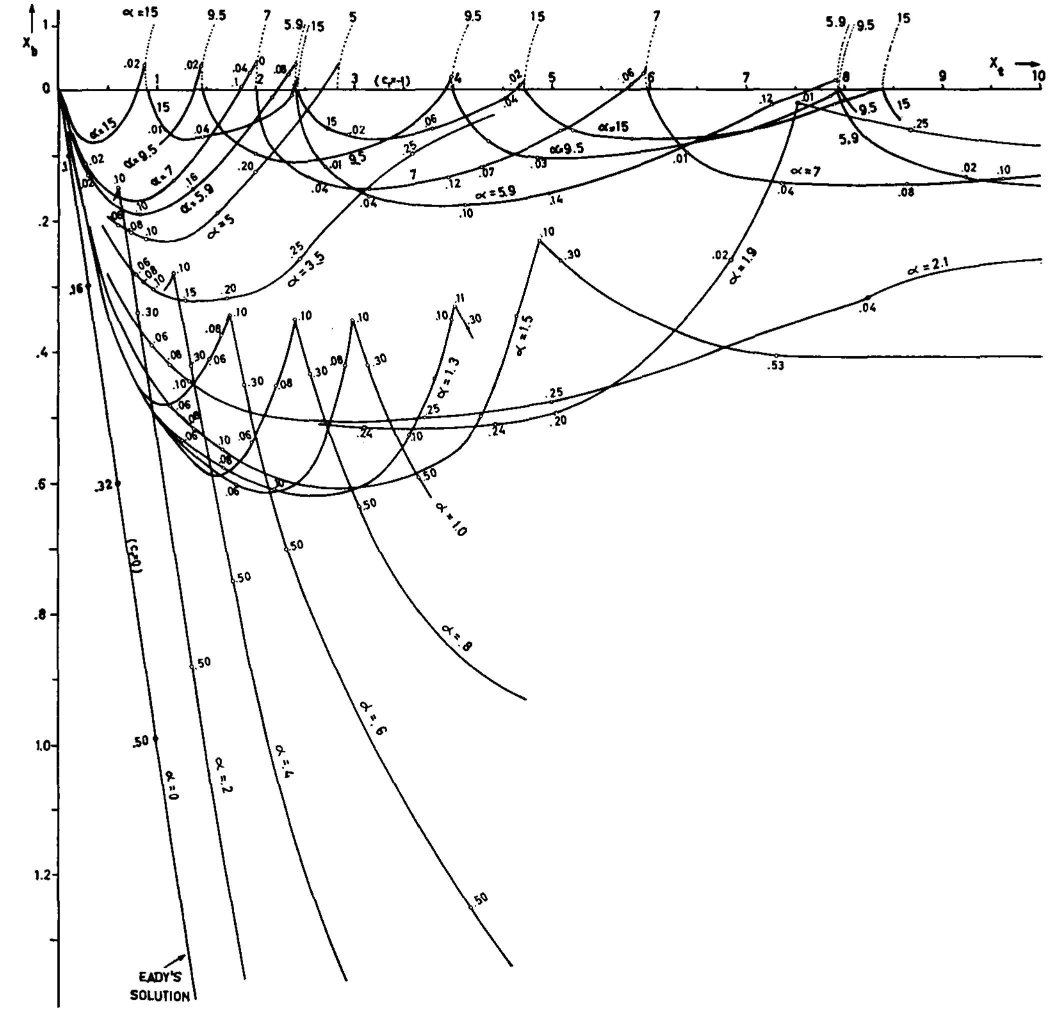

Fig. 4. Unstable solutions for various constant values of α. The figures on each line correspond to the growth rate X_i. The upper dotted lines ($X_b > 0$) are neutral solutions.

of the curves for the shortest wavelength is a result already found by Green (1960).

In the upper part of Fig. 4 (the quadrant $X_b \geqslant 0$, $X_t > 0$) the dotted lines represent neutral wave solutions for various values of α. This corresponds therefore to the lower part of Figs. 1 and 2, except that curves for new values of α have now been introduced.

The curves representing unstable solutions in Fig. 4 can be divided in two sets: those having a point of discontinuity in the derivative which does not reach the X_t-axis; and those that reach or intersect the X_t-axis. The two sets are separated by the critical value $\alpha = \alpha' \approx 3.3$ which corresponds to a curve which is tangent to the X_t-axis. It can be seen that for all values of $\alpha > \alpha'$ there is a continuous transition from the unstable to the neutral solutions. For $\alpha < \alpha'$ such a transition does not exist.

The meaning of these results can be more clearly seen in Figs. 6 and 7. Both contain the basic lines, regions and subregions of Fig. 3 with the addition of the isolines of the growth rate n for the unstable modes. Fig. 6 shows the n-lines for $\Lambda > 0.4$ and Fig. 7 the same for $\Lambda < 0.4$. In the latter it can be seen that in the b-region the growth rate isolines form closed unstable subregions which are bounded by the critical neutral lines. When $\lambda \to 0$ and $\Lambda \to 0$ these closed regions tend to be located between the lines $a = 0$, $a = -1$, $a = -2$, ..., etc. The growth rate $n \to 0$, in this limiting case on the lines where a is a negative integer or zero. Because of the definition of λ and Λ the limit $\lambda \to 0$, $\Lambda \to 0$ corresponds to Charney's model ($\dot{h} \to \infty$) and the results we have described agree with what has been demonstrated by Burger (1962) for that model, that is, there are no exponentially unstable solutions for negative integer values of a. As soon as Λ takes values different from zero, the unstable solutions expand toward the long waves, and we have conjugate complex roots even on the lines of negative integer values of a.

The parabola (6.3) boundary of the neutral roots is not a boundary of the unstable solutions and along the parabola the growth rate of the unstable roots does not vanish. This result differs from Green (1960) and Hirota (1968). That the parabola is not a line of zero growth rate for the unstable mode can be very clearly seen in Fig. 4 and it is simply a consequence of the fact already pointed out that no curve corresponding to values $\alpha < 2$ (which are the values defining the parabola) reach the X_t-axis.

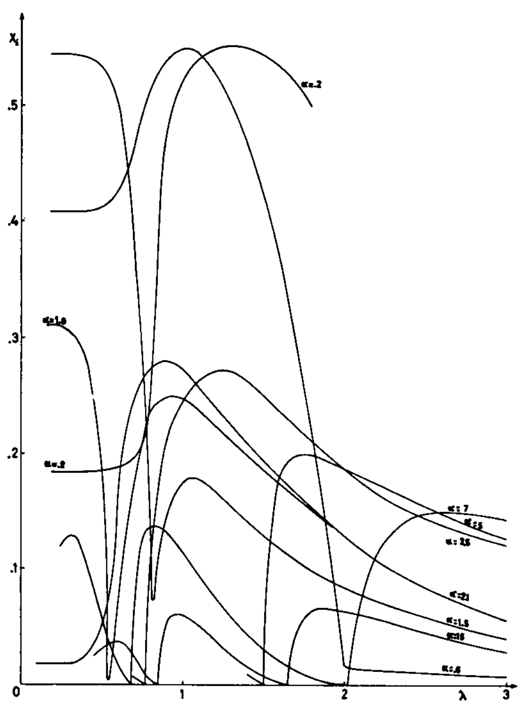

Fig. 5. Varation of X_i as a function of the dimensionless wavelength λ, for constant values of α.

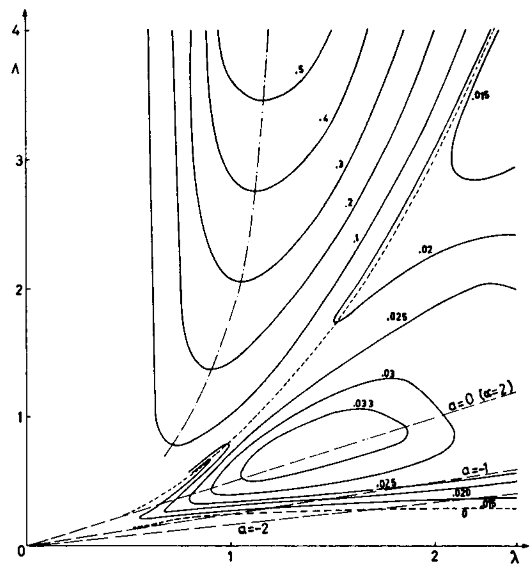

Fig. 6. Isopleths of the dimensionless growth rate n for large values of the shear ($\Lambda > 0.4$).

In Fig. 5, the variation of X_i (which is also a measure of the growth rate) with the nondimensional wavelength λ is represented for different values of the parameter α. A typical line for values $\alpha < 2$, such as $\alpha = 1.5$, protrudes downward towards the λ-axis but recurves without reaching it. Corresponding curves calculated by Green and Hirota actually reach the axis, a result which we believe is due to the numerical approximations they use in their calculations. This results, in their case, in points of zero growth rate for the unstable mode on the parabola (6.3).

If we consider the isoline $n = 0.001$ in the a-region of Fig. 7 we see that it comes down close to $a = -1$ (only a small section has been drawn), then goes up fairly close to $a = 0$, recurves, crosses the parabola and comes down close to it, recurves again near the origin and goes up again, parallel to the Λ-axis. A similar behaviour is suggested for the critical 0-line (of which only one segment has been represented), except that it should become the Λ-axis itself. A further indication of this fact can be obtained as follows. In Fig. 5 it can be seen that the value of X_i tends to keep approximately constant when $\lambda \to 0$. If we write the dimensionless growth rate n in the form:

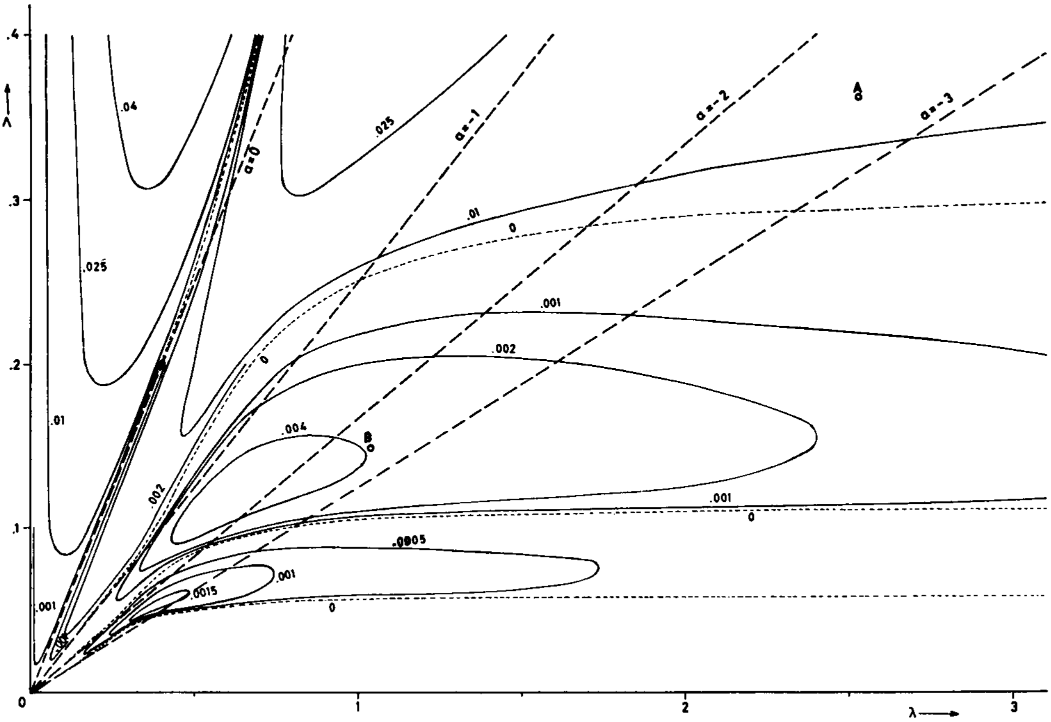

Fig. 7. Isopleths of the dimensionless growth rate n for small values of the dimensionless shear Λ.

$$n = \frac{X_t}{\alpha(X_t - X_b)} = \frac{X_t \lambda}{4\alpha}$$

we see that the growth rate is an approximately linear function of λ, on the lines of constant α, when $\lambda \to 0$. But, on the other hand, for the small values of $\alpha(\alpha < 1)$, and $\lambda \to 0$, the growth rate n becomes an approximately linear function of λ, because X_t/α becomes approximately constant as α decreases. It follows that n goes to zero as both λ and α go to zero, which means that the Λ-axis is a line $n = 0$.

Turning back to Fig. 4 we see that for all curves representing unstable modes, when $\alpha > \alpha'$, the transition from the unstable to the stable modes takes place at two different points on the neutral branch, according to whether we approach this branch, on the unstable curve, from increasing or decreasing values of X_t. This gap becomes still narrower towards the short waves (large X_t). We have computed the value of the gap for the curve $\alpha = 7$. The branch coming from larger values of X_t reaches the X_t-axis at a point X_t which corresponds to a wavelength $\lambda = 2.04$. The gap between the points of transition to neutral modes is $\Delta\lambda = 0.018$. The meaning of these gaps can be more easily seen in Fig. 7 as a narrow band of stable modes which separate contiguous b-subregions.

We should also notice (in Fig. 4) that, particularly for the long waves (i.e. small values of X_t), near the transition of the unstable solutions to the neutral waves, a pair of the unstable modes reaches a phase velocity slightly more retrograde than the speed of the surface undisturbed flow ($c_r < -1$).

The previous analysis of the characteristics of the several regions and subregions in the λ, Λ-diagram (Figs. 3, 6, 7) leads to the following results. The boundary between the a-region and the b-region is a critical line which becomes assymptotic to $\Lambda \approx 0.3$. For larger values of the non-dimensional shear there is a continuous transition from fast growing unstable modes to unstable modes with small growth rate. The eigenvalues of the characteristic equation of the model do not show the continuous transition from the conjugate complex roots as appears in the numerical computations of Green (1960) and Hirota (1968). On the other hand, for small

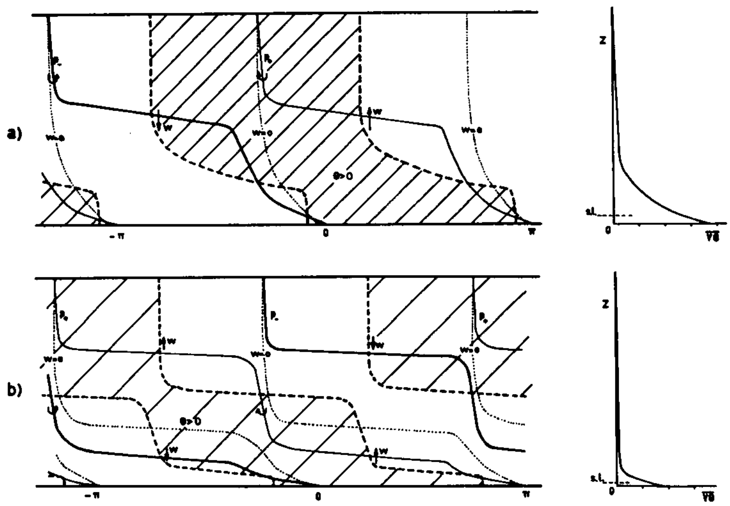

Fig. 8. Perturbation pressure field (full line), vertical velocity (dotted line) and potential temperature (dashed line), for (*a*) an unstable wave of the first *b*-subregion; (*b*) an unstable wave of the second *b*-subregion.

values of the shear ($\Lambda < 0.3$), a continuous transition from the unstable to stable solutions occurs if the value of the parameter a of the confluent hypergeometric equation is larger than a critical value.

8. The structure of unstable waves with small X_i

The vertical structure of the fields for the variables v, w, θ and p has been calculated for a large number of unstable waves at characteristic points of the λ, Λ diagram. Only two such waves have been reproduced in Fig. 8. They correspond to points A and B in Fig. 7. Fig. 8*a* corresponds to a wave in the first *b*-subregion. It shows the structure similar to that of a stable wave in middle and higher levels and of a baroclinic unstable wave at lower levels. In the second *b*-subregion (Fig. 8*b*) the unstable baroclinic region of the wave is still shallower. The vertical structure is considerably more complicated showing a double inversion of the sign of v with height, as well as an inversion in the sign of w.

The structure of the waves in other subregions becomes more and more complicated and the baroclinic zone reduces to a very shallow layer close to the lower boundary.

On the right side of Fig. 8 the variation of $\overline{v\theta}$ with height was plotted. We show below that the rate of "production" of eddy potential energy is proportional to $\overline{v\theta}$. It can be seen, Fig. 8*a* and *b*, that the maximum values of $\overline{v\theta}$ are concentrated in a layer which has the height of the baroclinic unstable region.

The conversion rate of energ ycan be calculated as follows. From equation (4.4):

$$\alpha - \frac{X}{2} + i\frac{X_i}{2} = \frac{\mu}{k}\frac{\partial}{\partial z}\left(\frac{W}{v}\right) + i\frac{g\mu}{f\bar{\theta}}\left(\frac{W\theta}{v^2}\right)$$

Horizontal ($\bar{\ }$) and vertical $\{\ \}$ averaging give:

$$\frac{(X_t - X_b)\, f^2 h}{2\mu^2 k U_0}\left[\alpha - \frac{X_t + X_b}{4} + i\frac{X_i}{2}\right] = i\overline{\left\{\frac{g}{\bar{\theta}}\left(\frac{W\theta}{v^2}\right)\right\}} \tag{8.1}$$

From (8.1), (5.1) and (5.9) one gets:

$$\delta\mu U_0 X_i = \overline{\left\{\frac{g}{\bar{\theta}}\left(\frac{W\theta}{v^2}\right)\right\}} \tag{8.2}$$

where $\delta = fU'/\sigma g$ is the slope of the isentropic surfaces in the unperturbed flow.

This relation (8.2) shows that X_i measures the efficiency of the conversion from potential into kinetic energy. This was already shown by Green (1960).

From the expression for the available potential energy (Lorenz, 1955):

$$\varrho = \frac{g}{2\sigma}\left(\frac{\theta}{\bar{\theta}}\right)^2 \tag{8.3}$$

we obtain, by using (3.3) multiplied by θ and horizontally averaged:

$$\frac{\partial \overline{\varrho}}{\partial t} = \frac{g}{\bar{\theta}}\,\overline{\delta v\theta} - \frac{g}{\bar{\theta}}\,\overline{w\theta} \tag{8.4}$$

On the other hand, the vorticity equation multiplied by v and horizontally averaged gives:

$$\frac{\partial \overline{K}}{\partial t} = \frac{f}{k^2}\frac{\partial}{\partial z}\overline{\left(v\frac{\partial w}{\partial x}\right)} + \frac{g}{\bar{\theta}}\,\overline{w\theta} \tag{8.5}$$

where $K = \frac{1}{2}v^2$ is the kinetic energy of the perturbation. We see that the second terms on the right-hand side of (8.4) and (8.5) measure the conversion of the eddy potential energy into eddy kinetic energy, whereas the first right-hand side term in (8.4) gives the rate at which the eddy potential energy is produced from the potential energy of the basic flow (given by the slope of the isentropics).

It seems, therefore, that the waves we are studying have the rate of production of eddy potential energy right at the layer which shows a typical unstable baroclinic structure.

It should be finally pointed out that the steering level is found within the baroclinic layer. The instability is not, however, necessarily associated with its presence. Unstable waves of similar structure, although exceptionally limiting cases, do not have steering level within the flow.

Acknowledgements

The authors express their gratitude to Susana Epstein, Silvia Selzer and Jöel Salas, for help in the programming for the computer and in the laborious work of computing and plotting. The computations were made by means of an IBM 360/40 of the Centro de Computacion of the Universidad de Chile.

REFERENCES

Bretherton, F. P. 1966*a*. Baroclinic instability and the short wavelength cut-off in terms of potential vorticity. *Quart. J. R. Met. Soc. 92,* 335–345.

Bretherton, F. P. 1966*b*. Critical layer instability in baroclinic flows. *Quart. R. J. Net. Soc. 92,* 325–334.

Burger, A. P. 1962. On the non-existence of critical wavelengths in a continuous baroclinic stability problem. *J. Atmos. Sci. 19,* 31–38.

Charney, J. G. 1947. The dynamics of long waves in a baroclinic westerly current. *J. Meteor. 4,* 135–163.

Eady, E. T. 1949. Long waves and cyclone waves. *Tellus 1,* 33–52.

Green, J. S. A. 1960. A problem in baroclinic instability. *Q.J.R.M.S. 86,* 237–251.

Hirota, I. 1968. On the dynamics of long and ultralong waves in a baroclinic zonal current. *J. Meteor. Soc. Japan 46,* 234–249.

Lorenz, E. 1955. Available potential energy and the maintenance of the general circulation. *Tellus 7,* 157–167.

Miles, J. W. 1964*a*. A note on Charney's model of zonal-wind instability. *J. Atmos. Sci. 21,* 451–452.

Miles, J. M. 1964*b*. Baroclinic instability of the zonal wind. *Rev. of Geophys. 2,* no. 1.

Miles, J. W. 1964*c*. Baroclinic instability of the zonal wind. Part. II. *J. Atmos. Sci. 21,* 500–506.

К ПРОБЛЕМЕ БАРОКЛИННОЙ НЕУСТОЙЧИВОСТИ

Проблема бароклинной неустойчивости зонального течения формулируется на основе предположений, аналогичных модели Грина. Динамические уравнения модели приводят к одному дифференциальному уравнению вырожденного гипергеометрического типа для вертикальной скорости. Решается задача на собственные значения, численные методы используются только для нахождения корней характеристического уравнения.

Показано, что для больших значений безразмерного сдвига Λ (который связан с параметом Грина $\gamma = 2\Lambda^{-1}$) существует непрерывный переход от быстро растущих неустойчивых мод к модам с малой скоростью роста. Собственные значения характеристического уравнения модели не указывают на непрерывный переход от комплексно сопряженных к действительным корням, как это имело место в численных результатах Грина (1960) и Хироты (1968). С другой стороны для меньших значений сдвига непрерывный переход от неустойчивых к устойчивым решениям может иметь место. На длинноволновом конце интервала неустойчивости имеются слабо неустойчивые волны, скорость которых находится вне пределов изменения скорости потока; на коротковолновом конце имеется небольшой провал в спектре неустойчивых волн.

При обсуждении структуры волн показано, что неустойчивые волны с небольшой скоростью возрастания имеют структуру бароклинно неустойчивых волн в мелком слое, прилегающем к нижней границе.